The Astrophysical Journal, 971:144 (8pp), 2024 August 20 https://doi.org/10.3847/1538-4357/ad6151

Scaling of Ion Bulk Heating in Magnetic Reconnection Outflows for the High-Alfvén-speed and Low-β Regime in Earth's Magnetotail

M. Øieroset[1], T. D. Phan[1], J. F. Drake[2], M. Starkey[3], S. A. Fuselier[3], I. J. Cohen[4], C. C. Haggerty[5], M. A. Shay[6], M. Oka[1], D. J. Gershman[7], K. Maheshwari[1,8], J. L. Burch[3], R. B. Torbert[9], and R. J. Strangeway[10]
[1] Space Sciences Laboratory, University of California, Berkeley, CA 94720, USA; oieroset@berkeley.edu
[2] University of Maryland, College Park, MD 20742, USA
[3] Southwest Research Institute, San Antonio, TX 78238, USA
[4] Johns Hopkins Applied Physics Laboratory, MD, USA
[5] University of Hawaii, Honolulu, HI, USA
[6] University of Delaware, DE, USA
[7] NASA Goddard Space Flight Center, Greenbelt, MD 20771, USA
[8] Now at Princeton University, Princeton, NJ 08544, USA
[9] Southwest Research Institute, Durham, NH 03824, USA
[10] University of California, Los Angeles, Los Angeles, CA 90095, USA
Received 2024 May 31; revised 2024 July 1; accepted 2024 July 8; published 2024 August 14

Abstract

We survey 20 reconnection outflow events observed by Magnetospheric MultiScale in the low-β and high-Alfvén-speed regime of the Earth's magnetotail to investigate the scaling of ion bulk heating produced by reconnection. The range of inflow Alfvén speeds (800–4000 km s^{-1}) and inflow ion β (0.002–1) covered by this study is in a plasma regime that could be applicable to the solar corona and flare environments. We find that the observed ion heating increases with increasing inflow (upstream) Alfvén speed, V_A, based on the reconnecting magnetic field and the upstream plasma density. However, ion heating does not increase linearly as a function of available magnetic energy per particle, $m_i {V_A}^2$. Instead, the heating increases progressively less as $m_i {V_A}^2$ rises. This is in contrast to a previous study using the same data set, which found that electron heating in this high-Alfvén-speed and low-β regime scales linearly with $m_i {V_A}^2$, with a scaling factor nearly identical to that found for the low-V_A and high-β magnetopause. Consequently, the ion-to-electron heating ratio in reconnection exhausts decreases with increasing upstream V_A, suggesting that the energy partition between ions and electrons in reconnection exhausts could be a function of the available magnetic energy per particle. Finally, we find that the observed difference in ion and electron heating scaling may be consistent with the predicted effects of a trapping potential in the exhaust, which enhances electron heating, but reduces ion heating.

Unified Astronomy Thesaurus concepts: Planetary magnetospheres (997); Solar magnetic reconnection (1504); Plasma physics (2089); Space plasmas (1544); Geomagnetic fields (646)

1. Introduction

Magnetic reconnection is a universal energy conversion process important in many space, astrophysical, and laboratory contexts, such as magnetospheric substorms, solar and stellar flares, and magnetic confinement fusion. The process converts stored magnetic energy into particle energy in the form of plasma jetting and heating.

Ion heating and its controlling factors is one of the key unresolved problems in reconnection research. Ion heating is observed in both laboratory reconnection (e.g., Ono et al. 1996; Hsu et al. 2000; Stark et al. 2005; Gangadhara et al. 2007; Yamada et al. 2010, 2014) and in space (e.g., Angelopoulos et al. 1992; Gosling et al. 2005; Ergun et al. 2020), but the degree of heating varies greatly. For example, reconnection exhausts at the magnetopause and in the solar wind show ion heating in the range of tens to a few hundred eV (Gosling et al. 1986, 2005, 2007; Phan et al. 2014; Wang et al. 2023), while reconnection exhausts in the Earth's magnetotail display ion heating up to tens of keV (e.g., Angelopoulos et al. 1992; Ergun et al. 2020), i.e., 2 orders of magnitude higher than at the magnetopause. These differences imply that ion heating in reconnection depends on the local plasma parameters.

Observational studies of the scaling of ion heating in reconnection in space have so far focused on the low-Alfvén-speed and large-β regimes of the solar wind and the magnetopause (Drake et al. 2009; Phan et al. 2014; Tilquin et al. 2020). These studies found that ion heating was linearly proportional to the inflowing available magnetic energy per particle (or inflowing Poynting flux per particle density flux), $m_i {V_A}^2$, with $\Delta T_i = 0.13\ m_i {V_A}^2$, where ΔT_i is increase in ion temperature from the inflow region to the exhaust, V_A is the inflow Alfvén speed, and m_i is the proton mass (Drake et al. 2009; Phan et al. 2014; Shay et al. 2014). This empirical relation predicts a degree of heating nearly a factor of 3 less than $m_i {V_A}^2/3$, which is the predicted heating arising from Alfvénic counterstreaming proton beams in the exhaust if the outflow speed is at the inflow Alfvén speed (Drake et al. 2009). This discrepancy is not fully understood but could be related to the observed outflow jets not always being fully Alfvénic (Haggerty et al. 2018).

Electron bulk heating in reconnection exhausts has also been found to be linearly dependent on $m_i {V_A}^2$, with $\Delta T_e = 0.017\ m_i {V_A}^2$ in the low-Alfvén-speed regime ($V_A < 600$ km s^{-1} and $\beta_e > 0.1$) at the magnetopause (Phan et al. 2013). Recently, Øieroset et al. (2023) reported that electron heating in the high-

Alfvén-speed ($V_A \sim$ 800–4000 km s^{-1}) and low-β ($\beta_e \sim$ 0.001–0.1) regime of Earth's magnetotail also increases linearly with the available magnetic energy per particle. They found that electron heating in reconnection exhausts follow the relation $\Delta T_e = 0.020\ m_i {V_A}^2$, implying that the magnetopause relation can be extrapolated to the magnetotail regime. If both ion and electron heating have the same functional form of dependency on $m_i {V_A}^2$, it can be deduced that the ratio of ion and electron heating is roughly a constant: $0.13/0.017 = 8$, using the magnetopause-derived heating relations (Phan et al. 2014).

However, other observations have suggested that the linear dependence of ion heating on $m_i {V_A}^2$ may not be universal, and that the ratio of ion-to-electron heating is not a constant. For example, in a study of reconnection ion diffusion regions in the large-Alfvén-speed and low-β magnetotail, Eastwood et al. (2013) found that on average, the ratio of ion-to-electron enthalpy flux was ~2.7. Laboratory experiments (Yamada et al. 2014) have found that 2/3 of magnetic energy is converted to ion energies, while 1/3 goes to electrons. These energies include kinetic energy flux, which is dominated by the ions, and the ratio of ion-to-electron heating in these laboratory studies was found to be approximately 1 to 1.

The nonuniversality of the linear dependence of heating on $m_i {V_A}^2$ has also been seen in theoretical simulations. Haggerty et al. (2015) explored the relative heating of ions and electrons in reconnection exhausts in PIC simulations and found that it is the sum of electron and ion heating that is linearly dependent on the available magnetic energy per particle, not electron and ion heating separately. This behavior was attributed to the presence of parallel electric fields and associated trapping potentials (Egedal et al. 2008, 2015) leading to multiple Fermi reflections for electrons, enhancing electron heating, but reducing ion heating by slowing the inflowing ions that make up the counterstreaming ion populations in the exhaust. The effects of the trapping potential may be different in different plasma regimes.

In this paper, we test the universality of the linear scaling relation for ion heating that was obtained from observational studies in the low-plasma-heating regime at the magnetopause (Phan et al. 2014). We do this by surveying reconnection events observed by Magnetospheric Multiscale (MMS) in the large-Alfvén-speed and low-β regime of the near-Earth magnetotail, in a plasma parameter regime that could be applicable to the solar environment. We also explore theoretical predictions of the impact of the electrostatic trapping potential on heating.

The paper is organized as follows. In Section 2 we describe the spacecraft instrumentation, and in Section 3 we present the database and event selection criteria. An event study is presented in Section 4 to illustrate the methodology. The statistical study is presented and discussed in Section 5, and the findings are summarized in Section 6.

2. Instrumentation

We use MMS Fast Survey mode data from the Earth's magnetotail between $X_{GSM} = -16.8\ R_E$ and $X_{GSM} = -27.5\ R_E$. We use magnetometer data at 8 samples per second (Russell et al. 2016) and electron moment and distribution data from the Fast Plasma Investigation (FPI) at 4.5 s resolution (Pollock et al. 2016). In the near-Earth magnetotail, the core and energetic tail of the ion distribution often span an energy range of ~100 eV to 100 keV. We therefore use proton data from the Hot Plasma Composition Analyzer (HPCA), with an energy range of ~10 eV to 40 keV, at 10 s resolution (Young et al. 2016), combined with proton observations from the Energetic Ion Spectrometer (EIS), which has an energy range of 45–500 keV and 20 s resolution (Mauk et al. 2016), to obtain combined proton moments of EIS and HPCA measured distributions.

The ion temperatures used in the present study are obtained by combining the moments of the HPCA and EIS proton distributions. A partial pressure tensor for each instrument is first computed in the spacecraft frame, which excludes normalization by ion density. The HPCA partial pressure tensor is interpolated to the time steps of EIS and then summed with the partial pressure tensor of EIS. The combined pressure tensor is computed by normalizing the combined partial pressure tensor by the combined HPCA and EIS ion density and transforming the result into the plasma rest frame (determined from the combined HPCA and EIS ion velocity). This pressure tensor is then converted to temperature units and diagonalized to produce the temperature tensor. The scalar temperature is then the trace of the temperature tensor and provides a measure of the average energy in the ion rest frame. We refer to these scalar temperatures as bulk temperatures and describe the increase in exhaust temperature (relative to the inflow temperature) as bulk heating.

The present study also uses electron temperatures from FPI, previously presented in Øieroset et al. (2023). FPI covers the energy range of the plasma sheet electron distribution well. Thus, plasma sheet electron temperature (i.e., the second moment of the electron distribution) is well measured by FPI. In the low-density lobe, on the other hand, the spacecraft potential is high, often making it challenging to accurately compute the moments of the electron distributions. The lobe electron temperature in this study is therefore obtained by Maxwellian fitting of the FPI electron distribution measurements averaged over the inflow interval (see Øieroset et al. 2023 for a more detailed description).

The observations are presented in the Geocentric Solar Magnetospheric (GSM) coordinate system, with the origin at the center of the Earth, positive X pointing toward the Sun, Y defined as the cross-product of the GSM X-axis and the magnetic dipole axis, and Z the cross-product of the X- and Y-axes. GSM is usually close to the coordinate system of the near-Earth magnetotail current sheet, with X being approximately along the reconnecting magnetic field (or outflow) direction, Z along the current sheet normal, and Y along the out-of-plane direction.

3. MMS Data Set and Event Selection Criteria

We utilize the list of magnetotail reconnection events from Øieroset et al. (2023), where the data set was used to study electron heating. The detailed selection criteria used to assemble these events are given in Øieroset et al. (2023) and summarized below.

This is a study of direct heating by reconnection in fully developed exhausts, i.e., downstream of the diffusion region, but away from the flow breaking region further downstream, where additional heating can occur (e.g., Runov et al. 2009; Barbhuiya et al. 2022). To avoid the flow breaking region, where other processes may contribute to heating, we focused on reconnection exhausts associated with tailward-to-earthward

flow reversals, which implies that the spacecraft is near a reconnection X-line moving tailward past the spacecraft. We avoided the diffusion region by selecting exhaust intervals where the outflow speed had stopped increasing and had reached a stable level. We also required the outflow interval to have a significant V_X component perpendicular to the magnetic field and $|B_X| < 10$ nT, which ensures the observations are obtained relatively close to the current sheet midplane, for fair comparisons between events.

For the inflow intervals we required that the interval should have a large and stable $|B_X| > 10$ nT, density less than the exhaust density, and be observed as close to the selected exhaust interval as possible. We also required an isotropic inflow electron temperature ($T_{e\|} \sim T_{e\perp}$) to ensure sampling of the asymptotic inflow, rather than the modified inflow where preheating of electrons takes place (Egedal et al. 2008; Chen et al. 2009; Shay et al. 2016).

In total, 21 events comprising 21 outflow/inflow intervals were selected for the magnetotail electron heating study (Øieroset et al. 2023). In the near-Earth magnetotail, reconnection can happen between plasma sheet field lines, and it can also progress to the lobe fields (e.g., Hones 1979; Baker et al. 2002; Cao et al. 2008; Oka et al. 2022). Both types are included in the data set. We use the same data set for the ion heating study, except for one 20 s duration exhaust event, where the ion outflow temperature was not well measured because of the low (20 s) resolution of the combined HPCA-EIS moments compared to the electron resolution. The 20 events are listed in Table 1. Magnetotail reconnection typically involves nearly symmetric inflow conditions and small guide magnetic field, usually <0.2 of the reconnecting field.

4. Sample Event

To illustrate the methodology used in the statistical study of ion bulk heating in magnetotail reconnection exhausts, Figure 1 shows MMS observations from 2017 July 17, when the spacecraft was in the plasma sheet at $XYZ_{GSM} = (-21.9, 6.8, 2.2)$ R_E. Between 14:38:30 UT and 14:41 UT the spacecraft encountered a high-speed tailward-directed reconnection jet (Figure 1(e)), followed by a region of large $|B_X|$ (Figure 1(a)) and lower density (Figure 1(g)). These observations suggest that the spacecraft encountered the reconnection inflow region.

We are interested in ion heating in the fully developed reconnection exhaust. Thus, we selected an outflow interval where the outflow jet has reached a stable level. Furthermore, to ensure a fair comparison between exhaust intervals from different events, we restricted the outflow observations to near the neutral sheet by requiring the outflow velocity to have a significant component perpendicular to the magnetic field (Figure 1(f)), and $|B_X| < 10$ nT (Figure 1(a)). The selected exhaust interval is marked with a pair of vertical red lines in Figure 1. The average exhaust temperature from the combined HPCA-EIS moments (Figure 1(h)) was 6623 eV.

Next, we identify an inflow interval that may be related to the reconnection outflow. As stated above, the spacecraft likely encountered the inflow region shortly after observing the reconnection jet. The inflow region should have large and stable $|B_X|$, density lower than the outflow, and isotropic inflow electron temperature ($T_{e\|} \sim T_{e\perp}$) to ensure sampling of the asymptotic inflow. The interval between the two vertical blue lines in Figure 1 satisfies these criteria. The relatively high inflow density of 0.086 cm^{-3} and ion temperature (4118 eV) indicate that the inflow in this event was plasma sheet plasma, not lobe. The inflow Alfvén speed was 1488 km s^{-1} and the inflow β_i was 0.36.

With the average ion temperature in the outflow interval being 6623 eV, the ion temperature increase, $\Delta T_i = T_{i,outflow} - T_{i,inflow}$ was 2505 eV. The electron heating, ΔT_e, for this event was 350 eV (Øieroset et al. 2023), i.e., the ion-to-electron heating ratio $\Delta T_i/\Delta T_{ie}$ was 7.2.

5. Statistical Study

Using the methodology explained in Section 3 and illustrated in the case study (Section 4), we examined the ion temperature change from inflow to outflow (ΔT_i) for the 20 large-Alfvén-speed reconnection events in Table 1 and studied how ΔT_i depends on plasma and field conditions in the inflow region. We also compared the magnetotail heating results with the low-Alfvén-speed findings from Phan et al. (2014), to investigate the universality of the ion heating scaling.

5.1. Statistical Findings of Ion Bulk Heating Dependence on Inflow Parameters

Figure 2(a) shows the ion temperature change from inflow to outflow, ΔT_i, versus the inflow Alfvén speed based on the X_{GSM} (roughly the reconnecting) component of the magnetic field ($V_{Ax,in}$) for the 20 magnetotail reconnection exhausts in the data set described above (Section 3, see also Table 1). For comparison, the dashed curve is the magnetopause-derived ion heating relation from Phan et al. (2014), $\Delta T_i = 1.34\ 10^{-3}\ {V_{Ax,in}}^2$, where ΔT_i is in units of eV and $V_{Ax,in}$ is in km s^{-1}. The observed ion heating increases with increasing Alfvén speed but does not follow the magnetopause-derived relation (dashed curve). Most data points are below the magnetopause-derived curve.

Ion heating also increases with the available magnetic energy per particle, $m_i {V_{Ax,in}}^2$ (Figure 2(b)). The data points appear to roughly follow the magnetopause relation ($\Delta T_i = 0.13\ m_i {V_{Ax,in}}^2$, dashed line) at low $m_i {V_{Ax,in}}^2$, but not at the highest energies where the data points are substantially below the magnetopause curve. A linear fit of the data (not shown) gives the relation $\Delta T_i = 0.073\ m_i {V_{Ax,in}}^2$ with a correlation coefficient of 0.75, which reflects the relatively large spread in the data.

We also examined how ΔT_i might depend on the individual inflow parameters N_{in}, $B_{x,in}$, and $T_{i,in}$. Figure 2(c) shows an inverse relationship between the temperature increase and the inflow density: events with large ion temperature increase (say >4 keV) generally have low inflow density (<0.06 cm^{-3}). In contrast, no discernible relationship is seen between ΔT_i and $|B_{x,in}|$ (approximately the reconnecting field) in this data set (Figure 2(d)). However, the range of $|B_{x,in}|$ in this data set (~15–30 nT) could be too small to reveal any dependency. Figure 2(e) shows that the highest ion heating events correspond to low inflow ion temperatures. Conversely, the highest ion inflow temperature events correspond to low ion heating. The latter is consistent with simulations by Haggerty et al. (2018), who found that high inflow temperature corresponds to lower outflow speed, which leads to reduced ion heating. However, this apparent relationship in the observations should be viewed with care, since the high heating events correspond to the inflows being in the low-density lobe, where the inflow ion temperature also tends to be low.

Table 1
List of Magnetotail Ion Heating Events

Event	Inflow Interval	Exhaust Interval	$\lvert B_{x,in}\rvert$ (nT)	N_{in} (cm^{-3})	$V_{Ax,in}$ (km s^{-1})	$\beta_{i,in}$	N_{out} (cm^{-3})	$T_{i,in}$ (eV)	$T_{i,out}$ (eV)	ΔT_i (eV)
1	2017-07-11/22:31:10-2017-07-11/22:32:00	2017-07-11/22:32:15-2017-07-11/22:33:15	11.6	0.051	1125	0.80	0.062	5289	5716	427
2	2017-07-11/22:38:47-2017-07-11/22:39:01	2017-07-11/22:36:59-2017-07-11/22:37:43	15.1	0.040	1641	0.39	0.151	5588	4759	−829
3	2017-07-17/07:50:25-2017-07-17/07:50:44	2017-07-17/07:48:02-2017-07-17/07:49:12	20.2	0.051	1931	0.34	0.066	6692	11516	4823
4	2017-07-17/14:43:11-2017-07-17/14:43:32	2017-07-17/14:39:12-2017-07-17/14:40:29	20.0	0.086	1488	0.36	0.204	4118	6623	2505
5	2017-07-17/14:43:11-2017-07-17/14:43:32	2017-07-17/14:46:18-2017-07-17/14:47:11	20.0	0.086	1488	0.36	0.207	4118	5336	1218
6	2017-07-26/00:13:03-2017-07-26/00:13:32	2017-07-26/00:18:04-2017-07-26/00:18:24	21.9	0.018	3909	0.0026	0.043	174	11660	11486
7	2017-07-26/13:00:16-2017-07-26/13:02:00	2017-07-26/13:05:22-2017-07-26/13:06:58	14.9	0.077	1172	0.97	0.082	7018	9620	2602
8	2017-08-23/14:44:12-2017-08-23/14:45:06	2017-08-23/14:49:59-2017-08-23/14:50:40	25.6	0.042	2728	0.013	0.141	492	11741	11250
9	2017-08-23/15:22:32-2017-08-23/15:23:30	2017-08-23/15:29:38-2017-08-23/15:33:00	28.1	0.058	2622	0.032	0.212	1076	8419	7344
10	2018-08-18/07:35:30-2018-08-18/07:36:27	2018-08-18/07:38:14-2018-08-18/07:39:18	20.9	0.035	2493	0.0057	0.219	177	7556	7379
11	2018-09-10/23:43:10-2018-09-10/23:43:42	2018-09-10/23:39:14-2018-09-10/23:39:44	32.3	0.23	1482	0.28	0.598	3173	5753	2580
12	2018-09-10/23:58:38-2018-09-10/23:59:02	2018-09-10/23:59:42-2018-09-11/00:01:24	26.1	0.32	1009	0.71	0.508	3795	4744	950
13	2019-08-05/15:54:16-2019-08-05/15:56:04	2019-08-05/15:52:08-2019-08-05/15:52:50	30.7	0.27	1290	0.29	0.570	2546	5492	2946
14	2019-08-05/16:17:42-2019-08-05/16:18:00	2019-08-05/16:19:25-2019-08-05/16:21:22	24.7	0.042	2691	0.048	0.222	1718	8146	6428
15	2019-08-08/14:01:37-2019-08-08/14:01:51	2019-08-08/13:57:50-2019-08-08/13:58:41	18.9	0.033	2285	0.0055	0.393	150	3444	3294
16	2019-08-08/14:06:24-2019-08-08/14:06:52	2019-08-08/14:15:48-2019-08-08/14:16:32	17.3	0.031	2128	0.0032	0.224	75	5305	5229
17	2019-08-12/14:21:26-2019-08-12/14:22:02	2019-08-12/14:19:54-2019-08-12/14:21:04	16.1	0.18	834	0.54	0.483	1955	3364	1409
18	2019-08-12/14:21:26-2019-08-12/14:22:02	2019-08-12/14:26:44-2019-08-12/14:27:48	16.1	0.18	834	0.54	0.513	1955	3156	1201
19	2019-09-08/16:21:42-2019-09-08/16:22:18	2019-09-08/16:17:24-2019-09-08/16:18:00	16.5	0.017	2773	0.012	0.094	485	4930	4445
20	2019-09-09/02:25:19-2019-09-09/02:25:44	2019-09-09/02:35:32-2019-09-09/02:36:40	17.2	0.010	3692	0.0027	0.108	191	4445	4254

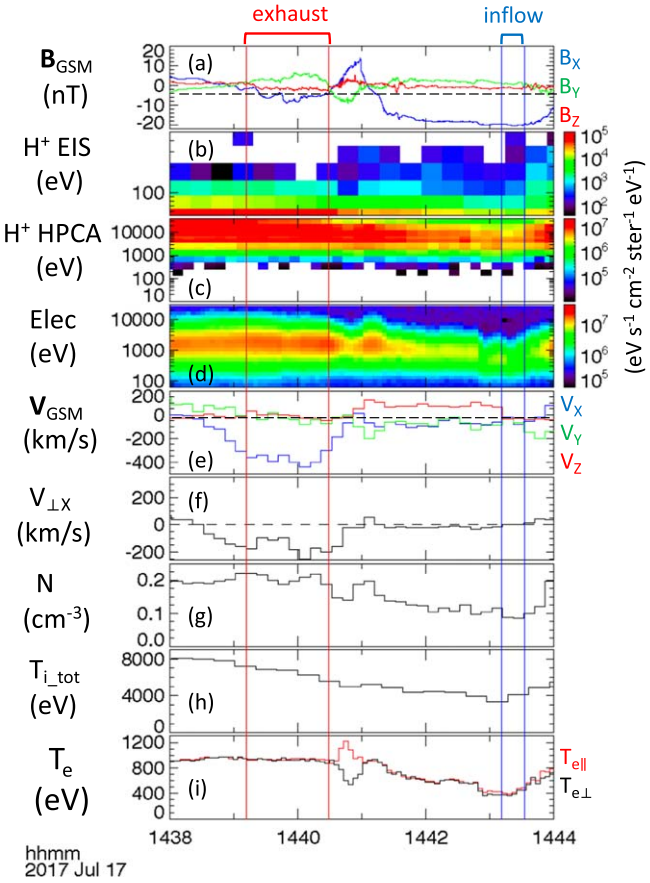

Figure 1. MMS observations of a magnetotail high-speed flow interval (red vertical lines) and the associated inflow (blue vertical lines). (a) Magnetic field components in GSM coordinates, (b) EIS proton spectrogram in differential energy flux, (c) HPCA proton spectrogram, (d) electron spectrogram, (e) proton velocity from HPCA, (f) perpendicular proton velocity along X_{GSM}, (g) proton density from HPCA, (h) total proton temperature from HPCA and EIS combined moments, and (i) electron temperature.

Figures 2(f) and (g) show ΔT_i versus inflow β_i and inflow β_e, respectively. The spread in the data is large, but in general the strongest ion heating is observed for small β_i and β_e.

We also investigated the relation between ΔT_i and ΔT_e (Figure 2(h)), using the electron heating values from Øieroset et al. (2023; which used the same data set). Not surprisingly, since ΔT_i does not depend linearly on $m_i V_{Ax,in}{}^2$ (Figure 2(b)) but ΔT_e does (Øieroset et al. 2023), the dependence between ΔT_i and ΔT_e is not linear. While the lowest heating events approximately follow the low-Alfvén-speed magnetopause relation $\Delta T_i \sim 8\ \Delta T_e$ (Phan et al. 2014; dashed line in Figure 2(h)), the ratio between ion and electron heating decreases with increasing heating. For large electron heating (~1000–3500 eV), the observed ion heating deviates significantly from the magnetopause-derived expression and $\Delta T_i/\Delta T_e$ is in the range 2–4.

5.2. Comparison with Theoretical Predictions of Ion Heating

As shown above, the relations between ΔT_i and $m_i V_A{}^2$ (Figure 2(b)) and ΔT_i and ΔT_e (Figure 2(h)), appear to approximately follow the magnetopause-derived linear expressions for low $m_i V_A{}^2$ and low ΔT_e values. For larger $m_i V_A{}^2$, ion heating appears to increase progressively less with increasing $m_i V_A{}^2$ and ΔT_e.

The observed reduction in ion heating has been predicted in theoretical studies. Haggerty et al. (2015) found that it is the sum of ion and electron heating, not the individual electron or ion heating, that is linearly dependent on the available magnetic energy per particle. Figure 3(a) displays the sum of the observed ion and electron heating versus the available magnetic energy per particle. The dashed line shows the magnetopause relation $\Delta T_i + \Delta T_e = (0.13 + 0.017)\ m_i V_{Ax,in}{}^2$ from adding the ion and electron heating relations in Phan et al. (2013, 2014). Indeed, adding ΔT_e to the ion heating appears to make the dependence on $m_i V_{Ax,in}{}^2$ more linear. A linear fit of the data results in the relation $\Delta T_i + \Delta T_e = 0.093\ m_i V_{Ax,in}{}^2$, with a correlation coefficient $R = 0.82$.

Haggerty et al. (2015) also predicted that a large-scale parallel electric field and its associated "trapping" potential (Egedal et al. 2008) controls the relative heating of electrons and ions in reconnection exhausts. The potential confines electrons in the exhaust, enabling them to undergo repeated Fermi reflections, which leads to enhanced electron heating (Egedal et al. 2008). At the same time the potential slows down ions entering the exhaust to below the Alfvén speed expected from the traditional counterstreaming picture of ion heating, leading to reduced ion heating. Haggerty et al. (2015) found the following relation between ion heating ΔT_i and the trapping potential $e\Delta\phi_n$:

$$\Delta T_i = \frac{1}{3} m_i V_0^2 - \frac{2}{3} e\Delta\phi_n, \tag{1}$$

where V_0 is the outflow speed in the reconnection exhaust and $e\Delta\phi_n$ is the potential. Haggerty et al. (2015) also provided a proxy for the potential:

$$e\Delta\phi_n \approx T_{e\|d} \ln(n_d/n_{\min}) \tag{2}$$

with e being the elementary charge, ϕ_n the potential across the exhaust, $T_{e\|d}$ the parallel electron temperature in the exhaust, n_d the maximum density in the exhaust, and $n_{\min}$ the minimum density, i.e., the inflow density.

While it is challenging to measure the potential directly, we use the proxy for the potential in Equation (2) and examine the observed $\Delta T_i + 2/3\ e\Delta\phi_n$ versus $m_i V_A{}^2$ (Figure 3(b)). The relationship appears to be more linear than the relation between ΔT_i and $m_i V_A{}^2$ (Figure 2(b)). Linear fitting gives $\Delta T_i + 2/3\ e\Delta\phi_n = 0.096\ m_i V_{Ax,in}{}^2$, with a correlation coefficient $R = 0.86$ (Figure 3(b)).

An approximate empirical expression for ion heating in the high-Alfvén-speed regime can then be obtained:

$$\Delta T_i \approx 0.1 m_i V_{Ax,in}{}^2 - 2/3 T_{e\|d} \ln(n_d/n_{\min}), \tag{3}$$

where we have substituted $e\Delta\phi_n$ with $T_{e\|d} \ln(n_d/n_{\min})$ from Equation (2). Equation (3) is similar to the theoretical expression in Equation (1), except for the 0.1 $m_i V_{Ax,in}{}^2$ term, which corresponds to $1/3\ m_i V_0^2$ in Equation (1). The smaller coefficient 0.1 in Equation (3) compared to $1/3$ in Equation (1) could perhaps be related to the use of V_A in Equation (3) instead of the outflow speed V_0 used in Equation (1). The reconnection outflow speed is generally less than the Alfvén speed in the magnetotail (Hau & Sonnerup 1989; Øieroset et al. 2000; Eriksson et al. 2004).

We use the observed V_A instead of the outflow speed V_0 because the observed outflow speed can be highly variable across the exhaust. This variability introduces significant

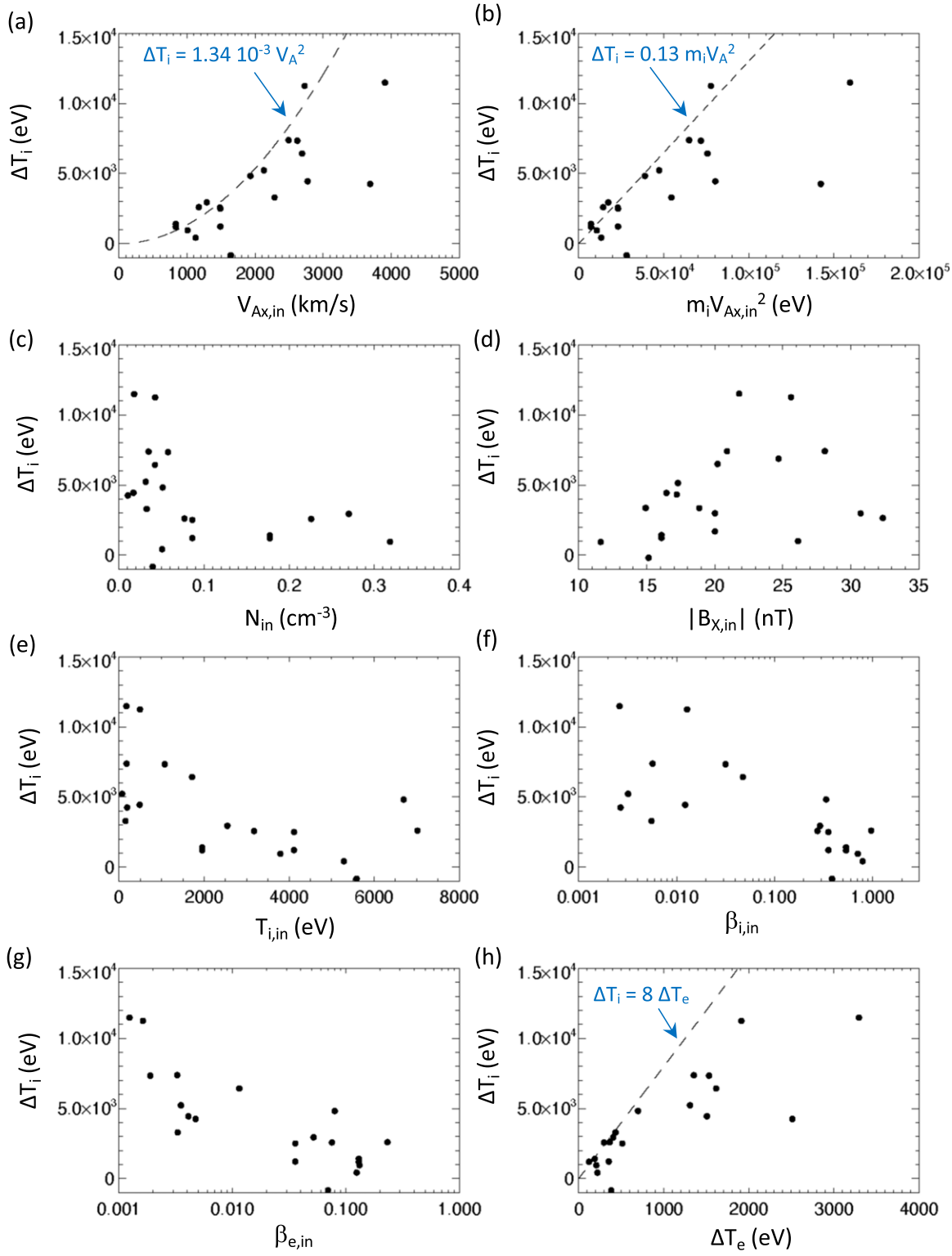

Figure 2. Ion heating ΔT_i vs. inflow parameters. (a) ΔT_i vs. inflow Alfvén speed based on the reconnecting field component B_X, (b) ΔT_i vs. available magnetic energy per particle, (c) ΔT_i vs. inflow density, (d) ΔT_i vs. inflow $|B_X|$, (e) ΔT_i vs. inflow ion temperature, (f) ΔT_i vs. inflow ion β, (g) ΔT_i vs. inflow electron β, and (h) ΔT_i vs. ΔT_e. Dashed curves in (a), (b), and (h) are the magnetopause-derived relations from Phan et al. (2014).

uncertainty in estimating an outflow speed. Using V_A also allows direct comparisons with the empirical magnetopause relation $\Delta T_i = 0.13\ m_i V_A{}^2$ (Phan et al. 2014).

One issue with Equation (3) is the relatively low correlation coefficient of 0.86, as is evident from the spread in the data in Figure 3(b). The factor $2/3$ in Equation (3) stems from the theoretical expression in Equation (1), but it is possible that this factor could vary. We therefore examined whether changing this factor could improve the fit. Figures 3(c) and (d) show the fits using the factors 1 and $3/2$ instead of $2/3$, which improves

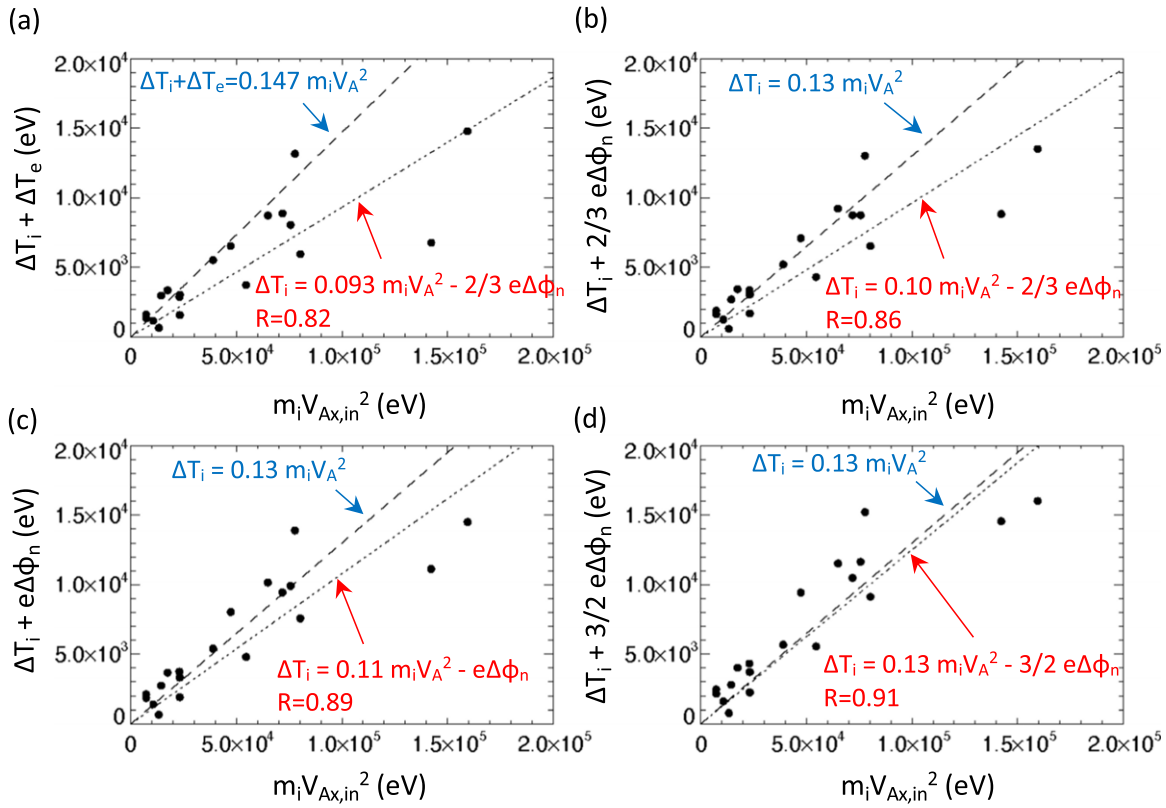

Figure 3. Comparisons with theoretical predictions for ion heating by Haggerty et al. (2015). (a) $\Delta T_i + \Delta T_e$ vs. $m_i V_A^2$, (b) $\Delta T_i + 2/3$ potential proxy (see text for details) vs. $m_i V_A^2$, (c) $\Delta T_i +$ potential proxy vs. $m_i V_A^2$, and (d) $\Delta T_i + 3/2$ potential proxy vs. $m_i V_A^2$. Dashed lines are the relations $\Delta T_i + \Delta T_e = 0.147\ m_i V_A^2$ (in panel (a)) and $\Delta T_i = 0.13\ m_i V_A^2$ (in panels (b)–(d)) derived from magnetopause exhausts in the low-Alfvén-speed regime (Phan et al. 2013, 2014). Dotted lines are linear fits of the data, with the resulting expression in red, including the correlation coefficient R.

the correlation coefficient to 0.89 and 0.91, respectively. Interestingly, the expression

$$\Delta T_i = 0.13\ m_i {V_{Ax,in}}^2 - 3/2 T_{e\|d} \ln(n_d/n_{min}) \quad (4)$$

results in a linear fit that is nearly identical to the magnetopause relation $\Delta T_i = 0.13\ m_i {V_{Ax,in}}^2$ (Figure 3(d)).

Equation (4) could provide a more general empirical expression for ion heating that is valid for both the low- and high-Alfvén-speed regime, at least up to $V_A = 4000$ km s^{-1}, which is the maximum Alfvén speed included in this study.

5.3. Sources of Uncertainty

As pointed out in the corresponding electron heating study (Øieroset et al. 2023), an important source of uncertainty comes from the fact that the outflow and inflow were not observed simultaneously, but with a delay of 1–9 minutes (Table 1). We assume that the inflow conditions remained stable for this length of time, but this stability is not known. To minimize this uncertainty, we selected only intervals where the outflow speed was stable for several minutes. Another source of uncertainty is the choice of inflow interval when two or more candidate inflow intervals were observed near an outflow interval. To be consistent, we choose the inflow interval that was observed closest to the selected outflow interval. The selected events (Table 1) constitute our best attempt to pair up inflow and outflow intervals.

6. Summary

We have performed a survey of ion heating in symmetric reconnection in the high-Alfvén-speed (800–4000 km s^{-1}) and low-inflow-β_i (0.002–1) regime of Earth's magnetotail, in a plasma parameter regime that could be applicable to the solar corona and flare environments, where the local Alfvén speed has been estimated to be ~2000–10,000 km s^{-1} (e.g., Phan et al. 2013; Chen et al. 2020). The magnetotail study extends a previous magnetopause reconnection study by 2 orders of magnitude in magnetic energy. We found that the ion heating increases with increasing inflow (upstream) Alfvén speed, V_A, based on the reconnecting magnetic field and the upstream plasma density. However, ion heating does not increase linearly as a function of available magnetic energy per particle (or Poynting flux per inflowing particle density flux), $m_i V_A^2$. Instead, the heating increases progressively less as $m_i V_A^2$ rises. This is in contrast to the finding of linear dependence of ion heating with $m_i V_A^2$ in the low-V_A and high-β regime at the magnetopause (Phan et al. 2014).

The ion heating behavior in the magnetotail exhausts (Figure 2(b)) is also markedly different from the reported electron heating in the same plasma regime (using the same data set), which was shown to increase linearly with $m_i V_A^2$ (Øieroset et al. 2023). Consequently, the ion-to-electron heating ratio $\Delta T_i/\Delta T_e$ also decreases as the heating increases (Figure 2(h)). Thus, the observations suggest that the energy partition between ions and electrons in reconnection exhausts could a be a function of the available magnetic energy per particle.

Interestingly, the ion-to-electron temperature ratio in Earth's magnetotail plasma sheet varies between 2 and 10 and has been found to decrease gradually with increasing temperature, reaching ratios of 2–5 for $T_i \sim 5$–10 keV (Wang et al. 2012). This gradual decrease in the plasma sheet temperature ratio could be related to the observed decrease in ion-to-electron heating ratio shown in Figure 2(h), suggesting that the plasma sheet ion and electron temperature could be controlled by magnetotail reconnection heating.

We compared the observational results with theoretical predictions by Haggerty et al. (2015) who found that the presence of a trapping potential in the reconnection exhaust (which increases electron heating), leads to reduced ion heating since the potential slows down ions entering the exhaust to below the Alfvén speed. While the potential is challenging to measure, we used a proxy for the potential provided by Haggerty et al. (2015), $e\Delta\phi_n \approx T_{e\|d} \ln(n_d/n_{\min})$, to compare the observations with the theoretical predictions. We found that the fit between $\Delta T_i + C\, e\Delta\phi_n$ (where C is a constant of order unity) and $m_i {V_{Ax,in}}^2$ is closer to being linear (Figures 3(b), (c), and (d)) than ΔT_i versus $m_i {V_{Ax,in}}^2$ (Figure 2(b)), suggesting that the observed reduction in ion heating for large $m_i {V_{Ax,in}}^2$ (Figure 2(b)) could indeed be caused by the presence of a trapping potential in the exhaust as proposed by Haggerty et al. (2015).

Acknowledgments

We would like to thank Shan Wang and Heli Hietala for helpful discussions. This research was supported by NASA grants 80NSSC18K1380, 80NSSC20K1781, NASA MMS contract NNG04EB99C (at SWRI), and NSF grant PHY-2409449 at UC Berkeley, NASA grant 80NSSC22K0352 and NSF grant PHY2109083 at the University of Maryland, and NASA grant 80NSSC20K0198 and NSF grant AGS-2024198 at the University of Delaware.

ORCID iDs

M. Øieroset https://orcid.org/0000-0003-3112-1561
T. D. Phan https://orcid.org/0000-0002-6924-9408
J. F. Drake https://orcid.org/0000-0002-9150-1841
I. J. Cohen https://orcid.org/0000-0002-9163-6009
C. C. Haggerty https://orcid.org/0000-0002-2160-7288
M. A. Shay https://orcid.org/0000-0003-1861-4767
M. Oka https://orcid.org/0000-0003-2191-1025
D. J. Gershman https://orcid.org/0000-0003-1304-4769
J. L. Burch https://orcid.org/0000-0003-0452-8403
R. B. Torbert https://orcid.org/0000-0001-7188-8690
R. J. Strangeway https://orcid.org/0000-0001-9839-1828

References

Angelopoulos, V., Baumjohann, W., Kennel, C. F., et al. 1992, JGR, 97, 4027
Baker, D. N., Peterson, W. K., Eriksson, S., et al. 2002, GeoRL, 29, 2190
Barbhuiya, M. H., Cassak, P. A., Shay, M., et al. 2022, JGRA, 127, e30610
Cao, X., Pu, Z. Y., Zhang, H., et al. 2008, JGRA, 113, A07S25
Chen, B., Shen, C., Gary, D. E., et al. 2020, NatAs, 4, 1140
Chen, L.-J., Bessho, N., Lefebvre, B., et al. 2009, PhPl, 16, 056501
Drake, J. F., Swisdak, M., Phan, T. D., et al. 2009, JGRA, 114, A05111
Eastwood, J. P., Phan, T. D., Drake, J. F., et al. 2013, PhRvL, 110, 225001
Egedal, J., Daughton, W., Le, A., & Borg, A. L. 2015, PhPl, 22, 101208
Egedal, J., Fox, W., Katz, N., et al. 2008, JGRA, 113, A12207
Ergun, R. E., Ahmadi, N., Kromyda, L., et al. 2020, ApJ, 898, 154
Eriksson, S., Øieroset, M., Baker, D. N., et al. 2004, JGRA, 109, A10212
Gangadhara, S., Craig, D., Ennis, D. A., et al. 2007, PhRvL, 98, 075001
Gosling, J. T., Eriksson, S., & Phan, T. D. 2007, GeoRL, 34, L06102
Gosling, J. T., Skoug, R. M., McComas, D. J., & Smith, C. W. 2005, JGRA, 110, A01107
Gosling, J. T., Thomsen, M. F., Bame, S. J., & Russell, C. T. 1986, JGR, 91, 3029
Haggerty, C. C., Shay, M. A., Chasapis, A., et al. 2018, PhPl, 25, 102120
Haggerty, C. C., Shay, M. A., Drake, J. F., Phan, T. D., & McHugh, C. T. 2015, GeoRL, 42, 065961
Hau, L.-N., & Sonnerup, B. U. Ö. 1989, JGR, 94, 6539
Hones, E.-W., Jr. 1979, SSRv, 23, 393
Hsu, S. C., Fiksel, G., Carter, T. A., et al. 2000, PhRvL, 84, 3859
Mauk, B. H., Blake, J. B., Baker, D. N., et al. 2016, SSRv, 199, 471
Øieroset, M., Phan, T. D., Lin, R. P., & Sonnerup, B. U. Ö. 2000, JGR, 105, 25247
Øieroset, M., Phan, T. D., Oka, M., et al. 2023, ApJ, 954, 118
Oka, M., Phan, T. D., Øieroset, M., et al. 2022, PhPl, 29, 052904
Ono, Y., Yamada, M., Akao, T., Tajima, T., & Matsumoto, R. 1996, PhRvL, 76, 3328
Phan, T. D., Drake, J. F., Shay, M. A., et al. 2014, GeoRL, 41, 7002
Phan, T. D., Shay, M. A., & Gosling 2013, GeoRL, 40, 4475
Pollock, C., Moore, T., Jacques, A., et al. 2016, SSRv, 199, 331
Runov, A., Angelopoulos, V., Sitnov, M. I., et al. 2009, GeoRL, 36, L14106
Russell, C. T., Anderson, B., Baumjohann, W., et al. 2016, SSRv, 199, 189
Shay, M. A., Haggerty, C. C., Phan, T. D., et al. 2014, PhPl, 21, 122902
Shay, M. A., Phan, T. D., Haggerty, C. C., et al. 2016, GeoRL, 43, 4145
Stark, A., Fox, W., Egedal, J., Grulke, O., & Klinger, T. 2005, PhRvL, 95, 235005
Tilquin, H., Eastwood, J. P., & Phan, T. D. 2020, ApJ, 895, 68
Wang, C.-P., Gkioulidou, M., Lyons, L. R., & Angelopoulos, V. 2012, JGRA, 117, A08215
Wang, R., Wang, S., Lu, Q., et al. 2023, NatAs, 7, 18
Yamada, M., Kulsrud, R., & Ji, H. 2010, RvMP, 82, 603
Yamada, M., Yoo, J., Jara-Almonte, J., et al. 2014, NatCo, 5, 5774
Young, D. T., Burch, J. L., Gomez, R. G., et al. 2016, SSRv, 199, 407